Published in final edited form as:
J Control Release. 2012 August 20; 162(1): 218–224. doi:10.1016/j.jconrel.2012.06.025.

Pulsed high intensity focused ultrasound increases penetration and therapeutic efficacy of monoclonal antibodies in murine xenograft tumors

Shutao Wang[a,b], **In Soo Shin**[c], **Hilary Hancock**[a], **Beom-su Jang**[c], **Hyung-sub Kim**[c], **Sang Myung Lee**[c], **Vesna Zderic**[b], **Victor Frenkel**[d], **Ira Pastan**[e], **Chang H. Paik**[c], and **Matthew R. Dreher**[a,*]

[a]Department of Radiology and Imaging Sciences, Clinical Center, National Institutes of Health, Bethesda, MD, United States

[b]Department of Electrical and Computer Engineering, George Washington University, Washington, DC, United States

[c]Division of Nuclear Medicine, Department of Radiology and Imaging Sciences, Clinical Center, National Institutes of Health, Bethesda, MD, United States

[d]Department of Biomedical Engineering, Catholic University of America, Washington, DC, United States

[e]Laboratory of Molecular Biology, Center for Cancer Research, National Cancer Institute, National Institutes of Health, Bethesda, MD, United States

Abstract

The success of radioimmunotherapy for solid tumors remains elusive due to poor biodistribution and insufficient tumor accumulation, in part, due to the unique tumor microenvironment resulting in heterogeneous tumor antibody distribution. Pulsed high intensity focused ultrasound (pulsed-HIFU) has previously been shown to increase the accumulation of ^{111}In labeled B3 antibody (recognizes Lewis^{y} antigen). The objective of this study was to investigate the tumor penetration and therapeutic efficacy of pulsed-HIFU exposures combined with ^{90}Y labeled B3 mAb in an A431 solid tumor model. The ability of pulsed-HIFU (1 MHz, spatial averaged temporal peak intensity = 2685 Wcm^{-2}; pulse repetition frequency = 1 Hz; duty cycle = 5%) to improve the tumor penetration and therapeutic efficacy of ^{90}Y labeled B3 mAb (^{90}Y-B3) was evaluated in Le^{y}-positive A431 tumors. Antibody penetration from the tumor surface and blood vessel surface was evaluated with fluorescently labeled B3, epi-fluorescent microscopy, and custom image analysis. Tumor size was monitored to determine treatment efficacy, indicated by survival, following various treatments with pulsed-HIFU and/or ^{90}Y-B3. The pulsed-HIFU exposures did not affect the vascular parameters including microvascular density, vascular size, and vascular architecture; although 1.6-fold more antibody was delivered to the solid tumors when combined with pulsed-HIFU. The distribution and penetration of the antibodies were significantly improved (p-value <

*Corresponding author at: National Institutes of Health, Building 10 Room 2N212 MSC1182, Bethesda, MD 20892, United States. Tel.: +1 301 402 8427; fax: +1 301 496 9933. dreherm@cc.nih.gov (M.R. Dreher).

0.05) when combined with pulsed-HIFU, only in the tumor periphery. Pretreatment with pulsed-HIFU significantly improved (p-value < 0.05) survival over control treatments.

Keywords

Monoclonal antibodies; Pulsed-HIFU; Radioimmunotherapy; Penetration; Binding site barrier

1. Introduction

Unlike traditional cancer therapies such as radiation or chemotherapeutics, monoclonal antibodies (mAb) are able to distinguish between normal and malignant tissue, thus potentially providing effective therapy while reducing negative side effects [1]. The development of monoclonal antibodies for cancer therapy over the last three decades has resulted in numerous FDA approved antibody-based therapies including tositumomab (Bexxar), ibritumomab tiuxetan (Zevalin) and rituximab (Rituxan) for hematological malignancies [2]. Despite progress in the treatment of hematological malignancies, the success and approval of antibody-based therapies that directly interact with a solid tumor cell are lacking with only 3 approved antibodies [3] including trastuzumab (Herceptin) for the treatment of breast cancer [4], cetuximab (Erbitux) for the treatment of colorectal cancer and head and neck cancer, and panitumumab (Vectibix) for the treatment of colorectal cancer [3]. The overall success in mAb therapy for direct treatment of solid tumors has been elusive.

The limited success in antibody therapy for solid tumors is primarily due to a number of factors, some of which are directly related to the abnormal characteristics of the tumor microenvironment. The relatively large size of mAbs (∼150 kDa) not only provides a long plasma half-life that is beneficial but also limits their extravasation due to reduced vascular permeability [2,5]. In contrast to normal tissues, tumors have an elevated interstitial fluid pressure (IFP), which may limit fluid filtration across the vessel wall and establish outward fluid motion from the tumor's periphery thus reducing tumor accumulation of convection-dominated macromolecules such as antibodies [6–8]. Once in the interstitium, antibodies have limited penetration due to specific interactions, such as the binding site barrier [9,10], and nonspecific interactions with components including extracellular matrix and cells [6,11,12]. All these factors combine to yield a heterogeneous distribution of antibodies in solid tumors [13,14].

In order to overcome these obstacles a number of potential solutions have been evaluated including single-chain antigen-binding proteins (sFvs) [15], immunotoxins [16], alternative protein scaffolds [17], alternative dosing schemes [18] and pretargeting approaches [19]. In addition to modifying the targeting agent, physiological modifiers that increase blood flow or vascular permeability through chemical (e.g. vasoactive agents) [20,21] or physical (e.g. hyperthermia) [22,23] means may improve antibody delivery. Recently ultrasound has been employed to improve antibody delivery [24–26].

Similar to light waves, ultrasound exposures can be focused in order to concentrate their energy, and hence raise their intensity in the focal zone. This higher intensity effectively

generates heat, elevating temperatures within seconds, to selectively ablate tissue by the process of coagulative necrosis. This ablative approach is commonly used to destroy tissue including prostate tumors and uterine fibroids under image guidance (ultrasound and magnetic resonance imaging [MRI]). The advantage of these high intensity focused ultrasound (HIFU) treatments is that the exposures are non-invasive, and can generally be carried out on an out-patient basis, with reduced cost and risk of infection compared to invasive surgical procedures [27]. Whereas continuous HIFU exposures are required to obtain high enough temperature elevations for ablating tissue (often > 60°C), pulsed-HIFU can be used to generate mild hyperthermic temperatures (39–44°C) due to their reduced rates of temporal energy deposition and because substantial cooling occurs between the pulses. In the absence of thermally destructive effects, non-thermal effects of ultrasound/ tissue interactions such as acoustic cavitation [28] and acoustic radiation forces [29] may be occurring to temporarily increase the permeability of the exposed tissue to enhance delivery [30].

Pulsed-HIFU exposures have been used to enhance the delivery of mAb-based agents. For example, transcranial ultrasound exposures with MRI guidance and a microbubble contrast agent demonstrated disruption of the blood brain barrier and a significant increase in trastuzumab delivery to the brain [25]. More recently, ultrasound exposures in combination with a microbubble contrast agent were used to enhance the delivery of anti-amyloid mAbs to the brain of plaque-bearing, transgenic mouse models of Alzheimer's disease possessing amyloid pathology [26]. In a flank tumor model with a human epidermoid carcinoma cell line (A431) expressing the Lewis^y antigen, commonly found in most human carcinomas, pulsed-HIFU exposures were given prior to the administration of an ^{111}In labeled B3 antibody, which is a murine IgG mAb that recognizes the Lewis^y antigen. The pulsed-HIFU exposures were found to more rapidly deliver the mAb to tumors and significantly enhanced the antibody delivery in terms of area under the curve [24].

The objective of this study was to investigate tumor penetration and therapeutic efficacy of pulsed-HIFU exposures combined with B3 mAb in an A431 solid tumor model. Fluorescently labeled mAbs and custom image processing of whole tumor sections were used to quantitatively analyze penetration from both the tumor surface/ periphery and blood vessel surface. Radiolabeled mAb was used to evaluate the therapeutic potential. The combination of pulsed-HIFU and radiolabeled mAb represents an image-guided, minimally invasive therapy that has potential to improve therapy of solid tumors by directly reducing the transport barriers that have limited the efficiency of antibody delivery for decades.

2. Materials and methods

2.1. Conjugation of Alexa-647 to B3

A fresh solution (7.44 mM) of succinimidyl ester of Alexa-647 (Invitrogen, Carlsbad, CA) dissolved in anhydrous DMSO was prepared. Immediately afterward, 90μl of this solution was added to 2.70 ml of B3 (66.7μM) dissolved in 0.25 M of sodium bicarbonate solution, pH 8.4. The solution was gently mixed and allowed to stand for 1 h at room temperature. The reaction mixture was analyzed by analytical size-exclusion HPLC (Gilson, Middleton, WI) equipped with a TSK gel G3000SW$_{XL}$ column (7.8×300 mm, 5μm, TOSOH

Bioscience, Japan; 0.067 M sodium phosphate/0.15 M sodium chloride, pH 6.8; 1.0 ml/min) and a UV/Visible monitor. The conjugation efficiency was then calculated by measuring the peak intensity of Alexa-647 conjugated B3 (Alexa-647-B3; retention time, 9.0 min) and unconjugated Alexa-647 (retention time, 12.5 min) at 650 nm. Alexa-647-B3 was purified with a size exclusion PD-10 column (GE Healthcare Bio-Sciences AB, Uppsala, Sweden) eluted with PBS.

2.2. Radiolabeling of mAb B3 with ^{90}Y

Radiolabeling with ^{90}Y was performed using a method reported previously [31]. Briefly, 10 mCi of $^{90}YCl_3$ (PerkinElmer, Boston, MA; 10 mCi/40μl of 0.05 M HC1) was adjusted to pH 4.2 with a 200 ml of buffer solution containing 0.30 M sodium acetate and 0.040 M sodium ascorbate in a polypropylene vial. Typically, 60μl of antibody conjugated with 2-(*p*-SCN-Bz)-6-methyl-DTPA (MX) (10.8 mg/ml, pH 7) was added and allowed to react at room temperature for 15 min at pH 4.2. To this reaction mixture, 30μl of 1 mM DTPA was added and the solution was incubated at room temperature for 5 min to complex any free ^{90}Y ions with DTPA. The radiolabeling yield was determined by instant thin layer chromatography with silica gel impregnated on glass fiber (ITLC; Gelman Sciences, Ann Arbor, MI) developed with 10% ammonium acetate in water:methanol (1:1). The radioactivity peak areas were integrated with a Bioscan radiochromatogram scanner (Bioscan Inc, Washington, DC). On ITLC, the radiolabeled antibody remains at the origin of application and ^{90}Y-DTPA moves with the solvent front. The labeled product, ^{90}Y-B3, was purified with a size exclusion PD-10 column (GE Healthcare Bio-Sciences AB) using PBS as the elution buffer. The radiochemical purity was assessed by measuring the percent peak intensity of ^{90}Y-B3 (retention time, 9.0 min) from HPLC (Gilson, Middleton, WI) equipped with a size exclusion TSK gel G3000SW$_{XL}$ column (7.8 × 300 mm, 5μm, TOSOH Bioscience, Japan; 0.067 M sodium phosphate/0.15 M sodium chloride, pH 6.8; 1.0 ml/min), a UV monitor and an on-line flow radioactivity detector (Bioscan Inc., Washington, DC). For the immunoreactivity determination, MX-B3 was labeled with ^{111}In at a specific activity of ∼ 10μCi/μg as described for the Y-90 labeling. Unconjugated B3 and Alexa-647-B3 were labeled with 4-[^{125}I] iodobenzoate [32] at a specific activity of ∼1.0μCi/μg. The iodinated B3 preparations were purified with a PD-10 column as described above.

2.3. Cell culture

A431, a human epidermoid carcinoma cell line that expresses the Lewis^y antigen recognized by B3, was grown in RPMI 1640 supplemented with 10% FCS, 2 mM L-glutamine, penicillin (100IU/ml), and streptomycin (100μg/ml) at 37°C in a humidified atmosphere with 5% CO_2. Cells were harvested with EDTA–trypsin, washed with PBS and resuspended in PBS with 1% BSA for immunoreactivity determination or resuspended in PBS for inoculation.

2.4. Cell-binding assay

The cell-binding assay was reported previously [32]. In brief, a constant concentration of ^{111}In-MX-B3 (5 ng, to evaluate the influence of MX labeling for ^{90}Y), ^{125}I labeled B3 (5 ng, as the B3 control) or ^{125}I labeled Alexa-647-B3 (5 ng, to evaluate the influence of Alexa-647-B3 labeling) was incubated with 2 × 10^4 to 2 × 10^6 of A431 cells for 2 h at 4°C.

Cell-bound radioactivity was separated by centrifugation and counted in a gamma counter. The percent maximum specific cell-bound radioactivity was used as the measure of immunoreactivity.

2.5. Tumor model

Animal experiments were performed under an NIH Animal Care and Use Committee approved protocol. Tumor xenografts were established by subcutaneous inoculation of 3×10^6 A431 cells in 0.1 ml PBS into the right hind flank of athymic mice (5–6 weeks, 18–20g; NCI-DCT, Frederick, MD).

2.6. HIFU system

All HIFU exposures were carried out using a custom built, image-guided, system, modified from a Sonoblate 500 (Focus Surgery, Indianapolis, IN). The probe comprises a spherical, concave 1 MHz therapeutic transducer (5 cm diameter; focal length 4 cm), and a co-axial, 10 MHz imaging transducer (8 mm aperture). The therapeutic transducer's focal zone was in the shape of an elongated ellipsoid, with an axial length (−3 dB intensity) of 7.2 mm and radial diameter (−3 dB intensity) of 1.38 mm.

2.7. Pulsed-HIFU exposures

Pulsed-HIFU exposures were carried out as previously described [24]. For all exposures, parameters were as follows: total acoustic power: 40 W (spatial averaged temporal peak intensity = 2685 Wcm^{-2}; peak rarefractional pressure=8.95 MPa); pulse repetition frequency: 1 Hz; duty cycle: 5% (50 ms ON; 950 ms OFF); 100 pulses at each raster point. Anesthetized mice were placed in a custom built holder and inserted vertically in to a bath of degassed water (for coupling), maintained at 36°C, where the head of the mouse was kept above the water. The holder was attached to a stage that could be manipulated in all three dimensions. With the imaging transducer in scanning mode, the mouse was positioned so that the tumor was directly within the focal zone of the therapeutic transducer. Once in position, a rastering sequence for treatment in the x and y plane was designated in a grid pattern, with a lateral (x) and vertical (y) spacing of 2 mm between raster points. On average, the HIFU procedure lasted 15 min depending on the tumor size. The mice in the control group were handled identically except with sham exposures (0W). Pulsed-HIFU exposures can provide a drug delivery benefit up to 24 h [33] but these effects gradually reverse to normal over 72 h [29]. Due to the long antibody circulation, they were administered within 10 min after pulsed-HIFU exposures.

2.8. Antibody penetration studies

Groups of tumor bearing mice (n = 4–5 mice/group) were injected with Alexa-647-B3 (150μg in 0.2 ml of PBS, *i.v.*) when the tumor size reached ∼200 mm^3. To investigate the effect of pulsed-HIFU, the tumor was first treated with pulsed-HIFU and the mice received Alexa-647-B3. Twenty four hours after the injection of Alexa-647-B3, the mice received a lateral tail vein injection of rhodamine-lectin (1 mg in 0.2 ml of PBS, RCA, Vector labs) to delineate functionally perfused blood vessels. Five minutes after the lectin injection, the mice were euthanized by CO_2 inhalation and exsanguinated by cardiac puncture. Tumors

were harvested with intact skin and flash-frozen using liquid nitrogen for subsequent tissue analysis.

2.9. Tissue analysis

Tumors were sectioned using a Leica CM1850 cryostat at 7μm thickness in 3 different regions to obtain representative sections throughout the tumor. Tumor sections were fixed with formalin for 20 min and mounted with Prolong Gold antifade reagent with DAPI (Invitrogen, Carlsbad, CA). Imaging was performed with a 10× objective (pixel size=1.29μm, binning 2×2) using an epi-fluorescent microscope (Zeiss, Axio Imager.M1, Thornwood, NY) equipped with a motorized scanning stage and mosaic stitching software (Axiovision, Zeiss). Three independent channels were obtained: DAPI for nuclei (shown in blue), Rhodamine for blood vessels (shown in red), and Cy5 for Alexa-647-B3 antibody (constant exposure time of 50 ms, shown in green). A tumor that did not contain Alexa-647-B3 antibody was imaged with identical parameters to obtain background signal intensity.

Image analysis was performed with a custom-designed MATLAB script (MathWorks, Natick, MA). Individual image channels were exported from Axiovision as 16-bit grayscale TIFF images to Photoshop (Adobe, San Jose, CA) where a tumor region was isolated to create a tumor mask. The tumor mask, blood vessel image and Alexa-647-B3 antibody image were loaded into MATLAB and a tumor blood vessel mask was created by segmenting the blood vessel image. Overall Alexa-647-B3 antibody intensity and penetration from the tumor edge and blood vessel surface (5μm bin size) were calculated with a background intensity subtraction. In addition, vascular parameters and architecture such as micro-vasculature density (MVD), blood vessel size, and median distance from a tumor pixel to the nearest vascular surface were measured. Values were grouped together from the 3 tumor regions to represent a tumor. Each tumor was treated as an independent sample (n=4–6).

2.10. Therapeutic studies

When the tumor size was ~200 mm^3, the mice received intravenous ^{90}Y-B3 alone (60μCi/ 150μg B3 in 0.2 ml of PBS). To investigate the effect of pulsed-HIFU on the radioimmunotherapy, the tumor was treated first with pulsed-HIFU and the mice received intravenous ^{90}Y-B3 (60μCi/ 150μg B3). Tumor dimensions and the body weight were measured daily for the first 3 or 4 days and thereafter, two or three times a week. The tumor volume was calculated by the following formula: $(a) \times (b)^2 \times 0.4$, where a is the longest dimension of the tumor and b is the tumor dimension perpendicular to it. Survival was defined as the day that the tumor volume exceeded 3× initial volume (after which the animal was euthanized) or the animal was euthanized for humane reasons (e.g., tumor exceeding maximum allowable size or excessive body weight loss). The experiment was repeated once and data pooled (n = 4–7 mice). Tumor volume versus time is displayed until the first day that the group became incomplete (euthanasia of the first animal in each group). Survival is displayed as a Kaplan–Meier plot and reported as median survival.

2.11. Statistics

All statistical analyses were performed in GraphPad Prism 5 (GraphPad Software, La Jolla, CA). Comparisons between two groups were performed with a *t*-test. Differences in penetration of antibody were compared by analyzing fluorescence intensity with a one way ANOVA followed by a Newman–Keuls post-hoc within 25 μm bins (larger bins than displayed to limit the number of statistical tests). Survival was displayed as a Kaplan–Meier plot with comparisons evaluated with a log-rank test. P-values less than 0.05 were considered statistically significant and all statistical tests were two-sided. Data are reported as mean±SEM unless otherwise indicated.

3. Results

3.1. Antibody labeling and immunoreactivity

The radiolabeling yield was >86% for both ^{90}Y- and ^{111}In-MX-B3 based on the percentage of the radioactivity associated between B3 and DTPA when analyzed by both ITLC and size exclusion HPLC methods. The conjugation yield of Alexa-647 to B3 was ∼ 70% when analyzed by size exclusion HPLC. The radiolabeled B3 and Alexa-647-B3 preparations with radiochemical purity and fluorescence purity of >98% were used for the in vitro and in vivo studies. The immunoreactivity of the radiolabeled B3 and Alexa-647-B3 used for the in vivo studies was >70%.

3.2. Microvascular analysis

Tumor sections were analyzed to determine the influence of pulsed-HIFU on the tumor microvasculature, as shown in Fig. 1. The microvascular density (MVD), distance from a tumor cell to the nearest vascular surface, and median blood vessel size were not significantly different between control and pulsed-HIFU treated tumors (p-value > 0.05, *t*-test).

3.3. Antibody accumulation and penetration

Antibody accumulation was determined by analyzing fluorescence intensity in whole tumor sections, as shown in Fig. 2 that qualitatively suggests that Alexa-647-B3 antibody (green) accumulation was improved with HIFU. Although not significant (p-value = 0.13), the antibody intensity in the entire tumor section was 1.6-fold greater in HIFU treated tumors (see Fig. 1D). More antibodies were consistently found in the tumor periphery, near the tumor surface, and in areas of greater vascular density. Quantitative analysis of the intensity of antibody from the tumor surface, as shown in Fig. 3A, demonstrated high intensity near the tumor surface that increased slightly over tens of microns then diminished drastically (5- to 8-fold) only 1 mm from the tumor surface. HIFU significantly (p-value < 0.05, Newman–Keuls) improved the amount of antibody within 50 μm of the tumor surface (except at the tumor surface, 0 μm). It is important to note that the amount of antibody in the tumor core (i.e., greater than ∼200 μm of the tumor surface) is very similar between groups. The antibody concentration diminished with distance from the blood vessel surface as shown in Fig. 3B. Although there is a greater antibody concentration with HIFU exposure in the vicinity surrounding each blood vessel, this difference was not significant (p-value > 0.05, Newman– Keuls).

3.4. Antitumor efficacy

Efficacy of ^{90}Y-B3 in combination with HIFU was determined by monitoring tumor growth after a single treatment, as shown in Fig. 4. Median survival was not significantly different between control, HIFU, and ^{90}Y-B3 corresponding to 3.5, 4 and 4 days, respectively (p-value > 0.05). Treatment with ^{90}Y-B3+ HIFU extended median survival to 19 days, significantly longer than treatment with ^{90}Y-B3 alone (p-value = 0.0007).

4. Discussion

HIFU is increasingly being used to improve drug delivery to solid tumors in preclinical studies [30]. The objective of this study was to investigate the tumor penetration and therapeutic efficacy of pulsed-HIFU exposures combined with B3 mAb in a solid tumor model. The pulsed-HIFU exposures did not appear to affect the vascular parameters measured here including MVD, vascular size, and vascular architecture (see Fig. 1). Despite these consistent vascular properties, 1.6-fold more antibody was delivered to solid tumors (see Fig. 1D and Fig. 3) when combined with pulsed-HIFU consistent with a previous report that demonstrated 2.1-fold greater %ID/g of B3 antibody following pulsed-HIFU exposures [24]. However, this previous study did not provide any mechanistic understanding or demonstrate improved efficacy of this strategy. In addition to delivery, the distribution and penetration of the antibodies were improved when combined with pulsed-HIFU only in the tumor periphery resulting in improved efficacy.

Although often cited as a key therapeutic barrier in antibody-based therapies, the concept of antibody penetration is more challenging to define or to quantitatively address [34]. The penetration of agents in a solid tumor can be operationally defined at different length scales as: 1) penetration from the surface of the tumor boundary into the tumor center (whole tissue scale), 2) penetration across the tumor blood vessel (apparent vascular permeability), 3) penetration away from the blood vessels through the interstitial space (analogous to the effective diffusion coefficient), and 4) penetration into the tumor cell itself (cellular uptake) [35].

Antibodies are macromolecules, and are classically thought of as convection dominated (meaning that they require fluid flow for transport). Therefore, antibodies would require net fluid filtration across the blood vessel wall to substantially accumulate in a tumor interstitium [6]. Examining the images in Fig. 2 would suggest that more transvascular transport occurred in the tumor periphery than the tumor core despite the presence of functionally perfused vessels throughout the tumor. The transvascular pressure gradient (both hydrostatic and osmotic) must be more favorable for extravasation in the tumor periphery than tumor core to produce this peripheral antibody distribution. In fact, interstitial fluid pressure (IFP) is often elevated in solid tumors but declines in the tumor periphery in the outer 0.2–1.1 mm [7], similar to the region of enhanced antibody delivery (see Fig. 2). If the osmotic pressure gradient is relatively constant throughout the tumor, then a reduction in IFP may have caused the enhanced antibody delivery to the tumor periphery. This enhanced delivery may be considered a form of improved penetration but this phenomenon is dominant only in the tumor periphery.

Further investigation is warranted into the manner by which pulsed-HIFU exposures may generate effects on the tumor microenvironment to facilitate the delivery of antibodies. The HIFU mechanisms for producing bioeffects are generally classified into thermal and non-thermal, where the latter includes acoustic cavitation and acoustic radiation forces [36]. Mild hyperthermia (40–42°C), as was previously shown to occur in murine flank tumors using pulsed-HIFU exposures similar to those used in the present study [37,38], has been shown to improve antibody delivery but would require heating durations up to 4 h for enhanced accumulation [23], considerably longer than the 100 s per treated raster point used in the present study. Both acoustic cavitation and radiation force induced bioeffects have been demonstrated with the high pressures and intensities used herein [33] that may lead to increased permeability of tissue to solutes [39]. Cavitation effects are generally restricted to the vasculature due to the requirement of available gas and physical space for bubble formation and growth [28]. On the other hand, acoustic radiation force induced displacements that result in locally generated shear strain may increase effective pore size of tissue. In skeletal muscle in a murine flank, pulsed-HIFU exposures increased gap size between muscle fiber bundles and disrupted collagen in the extracellular matrix (ECM) that coincided with improved distribution of locally administered nanoparticles [29]. The increase in permeability of tissue to solutes implies that the hydraulic conductivity (ease with which water moves) of tissue may also be increased. The generation of similar effects in tumors in the present study with the pulsed-HIFU exposures may have increased the hydraulic conductivity of the interstitial space, leading to lower IFP in the periphery [40], and increased the apparent vascular permeability [41]. These combined effects may have caused the improved antibody accumulation and distribution, especially in the tumor periphery. However, any IFP reduction was not sufficient to improve delivery to the tumor core.

Pre-exposure of the tumors to pulsed-HIFU prior to the administration of ^{90}Y-B3 resulted in significantly improved growth delay and survival. It is possible that the pulsed-HIFU exposures modified the biology of the cancer cells (i.e., mechanotransduction) making them more susceptible to radiation. However, it is more likely that the increased accumulation of antibodies provided a greater dose of radiation to the tumor directly. Since most of the accumulation was in the tumor periphery, this must have been sufficient for improved therapy. This highlights an inherent advantage of radioimmunotherapy with ^{90}Y of solid tumors over other forms of antibody therapy in that all tumor cells are not required to interact with the antibody. The ^{90}Y-labeled antibody is capable of exerting its therapeutic effect at a distance from the antibody itself (mean penetration = 2.4 mm, max penetration=11 mm). The preferential accumulation in the tumor periphery may irradiate all tumor cells through the concept of “crossfire” where cells in the tumor center are irradiated by a distant source, which is likely with ^{90}Y [42]. However this approach may become more problematic with larger tumors with insufficient radiation crossfire.

In addition to pulsed-HIFU, other methods may improve delivery of macromolecules, such as antibodies, to solid tumors. The emergence of iRGD has potential to improve the delivery and penetration of macromolecular cargo through a neuropilin-1-dependent manner [43]. Pretreatment with chemotherapeutics can subsequently improve the delivery of a second agent [44]. Enzymes may also modify the ECM to improve penetration of therapeutic agents

[45,46]. Multistage delivery platforms that “shrink” once localized to a tumor to improve penetration represent and interesting recent advance [47]. Improved nanoparticle penetration is highly dependent on nanoparticle properties and pulsed-HIFU exposures parameters as has been demonstrated in breast cancer spheroids [48]. However, the penetration of affinity targeted macromolecules may always be limited by the binding site barrier, depending on the affinity and receptor density, which does not seem to be alleviated by pulsed-HIFU.

Radioimmunotherapy has ample room for improvement and optimal combinations with pulsed-HIFU may require further investigations. Only one antibody, dose, and time point was examined which cannot capture the entire dynamic process. The dose, administration timing, and affinity of an antibody as well as the antigen expression density may also influence its distribution and heterogeneity [14]. Additional time points may better elucidate the process of antibody accumulation but the time point of maximal accumulation [24] was used in this study. The sequencing of pulsed-HIFU and antibody was based on previous studies but may require further refinement or even the use of multiple pulsed-HIFU exposures to optimize this strategy.

The use of HIFU in the clinic, mostly for ablation of benign (uterine fibroids) and malignant (prostate) tumors, is becoming more routine in clinical practice [27]. It may be possible to sufficiently improve the delivery of antibodies in combination with pulsed-HIFU to make previously ineffective antibodies more therapeutically efficacious. Combination strategies, such as presented here, may be the key to improving antibody efficacy in the clinic.

5. Conclusions

Pretreatment with pulsed-HIFU resulted in significantly improved B3 antibody penetration, only in the tumor periphery, and improved survival.

Acknowledgments

This research was supported by in part by the Intramural Research Program of the National Institutes of Health (NIH), Center for Interventional Oncology, National Cancer Institute, and Center for Cancer Research. We thank Dr. Bradford J. Wood for his useful discussion and support of this study.

References

1. Allen TM. Ligand-targeted therapeutics in anticancer therapy. Nat Rev Cancer. 2002; 2:750–763. [PubMed: 12360278]
2. Koppe MJ, Postema EJ, Aarts F, Oyen WJ, Bleichrodt RP, Boerman OC. Antibody-guided radiation therapy of cancer. Cancer Metastasis Rev. 2005; 24:539–567. [PubMed: 16408161]
3. Yan L, Hsu K, Beckman RA. Antibody-based therapy for solid tumors. Cancer J. 2008; 14:178–183. [PubMed: 18536557]
4. Slamon DJ, Leyland-Jones B, Shak S, Fuchs H, Paton V, Bajamonde A, Fleming T, Eiermann W, Wolter J, Pegram M, Baselga J, Norton L. Use of chemotherapy plus a monoclonal antibody against HER2 for metastatic breast cancer that overexpresses HER2. N Engl J Med. 2001; 344:783–792. [PubMed: 11248153]
5. Jain M, Venkatraman G, Batra SK. Optimization of radioimmunotherapy of solid tumors: biological impediments and their modulation. Clin Cancer Res. 2007; 13:1374–1382. [PubMed: 17309914]

6. Jain RK, Baxter LT. Mechanisms of heterogeneous distribution of monoclonal antibodies and other macromolecules in tumors: significance of elevated interstitial pressure. Cancer Res. 1988; 48:7022–7032. [PubMed: 3191477]
7. Boucher Y, Baxter LT, Jain RK. Interstitial pressure-gradients in tissue-isolated and subcutaneous tumors—implications for therapy. Cancer Res. 1990; 50:4478–4484. [PubMed: 2369726]
8. Heldin CH, Rubin K, Pietras K, Ostman A. High interstitial fluid pressure—an obstacle in cancer therapy. Nat Rev Cancer. 2004; 4:806–813. [PubMed: 15510161]
9. Weinstein JN, Eger RR, Covell DG, Black CDV, Mulshine J, Carrasquillo JA, Larson SM, Keenan AM. The pharmacology of monoclonal-antibodies. Ann N Y Acad Sci. 1987; 507:199–210. [PubMed: 3327413]
10. Saga T, Neumann RD, Heya T, Sato J, Kinuya S, Le N, Paik CH, Weinstein JN. Targeting cancer micrometastases with monoclonal antibodies: a binding-site barrier. Proc Natl Acad Sci U S A. 1995; 92:8999–9003. [PubMed: 7568060]
11. Jain RK. Vascular and interstitial barriers to delivery of therapeutic agents in tumors. Cancer Metastasis Rev. 1990; 9:253–266. [PubMed: 2292138]
12. Jain RK. Physiological barriers to delivery of monoclonal antibodies and other macromolecules in tumors. Cancer Res. 1990; 50:814s–819s. [PubMed: 2404582]
13. Baker JH, Lindquist KE, Huxham LA, Kyle AH, Sy JT, Minchinton AI. Direct visualization of heterogeneous extravascular distribution of trastuzumab in human epidermal growth factor receptor type 2 overexpressing xenografts. Clin Cancer Res. 2008; 14:2171–2179. [PubMed: 18381959]
14. Lee CM, Tannock IF. The distribution of the therapeutic monoclonal antibodies cetuximab and trastuzumab within solid tumors. BMC Cancer. 2010; 10:255. [PubMed: 20525277]
15. Yokota T, Milenic DE, Whitlow M, Schlom J. Rapid tumor penetration of a single-chain Fv and comparison with other immunoglobulin forms. Cancer Res. 1992; 52:3402–3408. [PubMed: 1596900]
16. Pastan I, Hassan R, Fitzgerald DJ, Kreitman RJ. Immunotoxin therapy of cancer. Nat Rev Cancer. 2006; 6:559–565. [PubMed: 16794638]
17. Zahnd C, Kawe M, Stumpp MT, de Pasquale C, Tamaskovic R, Nagy-Davidescu G, Dreier B, Schibli R, Binz HK, Waibel R, Pluckthun A. Efficient tumor targeting with high-affinity designed ankyrin repeat proteins: effects of affinity and molecular size. Cancer Res. 2010; 70:1595–1605. [PubMed: 20124480]
18. DeNardo GL, Schlom J, Buchsbaum DJ, Meredith RF, O'Donoghue JA, Sgouros G, Humm JL, DeNardo SJ. Rationales, evidence, and design considerations for fractionated radioimmunotherapy. Cancer. 2002; 94:1332–1348. [PubMed: 11877764]
19. Goldenberg DM, Sharkey RM, Paganelli G, Barbet J, Chatal JF. Antibody pretargeting advances cancer radioimmunodetection and radioimmunotherapy. J Clin Oncol. 2006; 24:823–834. [PubMed: 16380412]
20. Netti PA, Hamberg LM, Babich JW, Kierstead D, Graham W, Hunter GJ, Wolf GL, Fischman A, Boucher Y, Jain RK. Enhancement of fluid filtration across tumor vessels: implication for delivery of macromolecules. Proc Natl Acad Sci U S A. 1999; 96:3137–3142. [PubMed: 10077650]
21. Folli S, Pelegrin A, Chalandon Y, Yao X, Buchegger F, Lienard D, Lejeune F, Mach JP. Tumor-necrosis factor can enhance radio-antibody uptake in human colon carcinoma xenografts by increasing vascular permeability. Int J Cancer. 1993; 53:829–836. [PubMed: 8449608]
22. Kinuya S, Yokoyama K, Michigishi T, Tonami N. Optimization of radio-immunotherapy interactions with hyperthermia. Int J Hyperthermia. 2004; 20:190–200. [PubMed: 15195513]
23. Hauck ML, Dewhirst MW, Bigner DD, Zalutsky MR. Local hyperthermia improves uptake of a chimeric monoclonal antibody in a subcutaneous xenograft model. Clin Cancer Res. 1997; 3:63–70. [PubMed: 9815539]
24. Khaibullina A, Jang BS, Sun H, Le N, Yu S, Frenkel V, Carrasquillo JA, Pastan I, Li KC, Paik CH. Pulsed high-intensity focused ultrasound enhances uptake of radiolabeled monoclonal antibody to human epidermoid tumor in nude mice. J Nucl Med. 2008; 49:295–302. [PubMed: 18199622]

25. Kinoshita M, McDannold N, Jolesz FA, Hynynen K. Noninvasive localized delivery of Herceptin to the mouse brain by MRI-guided focused ultrasound-induced blood-brain barrier disruption. Proc Natl Acad Sci U S A. 2006; 103:11719–11723. [PubMed: 16868082]
26. Raymond SB, Treat LH, Dewey JD, McDannold NJ, Hynynen K, Bacskai BJ. Ultrasound enhanced delivery of molecular imaging and therapeutic agents in Alzheimer's disease mouse models. PLoS One. 2008; 3:e2175. [PubMed: 18478109]
27. Kennedy JE. High-intensity focused ultrasound in the treatment of solid tumours. Nat Rev Cancer. 2005; 5:321–327. [PubMed: 15776004]
28. Hynynen K. Focused ultrasound for blood-brain disruption and delivery of therapeutic molecules into the brain. Expert Opin Drug Deliv. 2007; 4:27–35. [PubMed: 17184160]
29. Hancock HA, Smith LH, Cuesta J, Durrani AK, Angstadt M, Palmeri ML, Kimmel E, Frenkel V. Investigations into pulsed high-intensity focused ultrasound-enhanced delivery: preliminary evidence for a novel mechanism. Ultrasound Med Biol. 2009; 35:1722–1736. [PubMed: 19616368]
30. Frenkel V. Ultrasound mediated delivery of drugs and genes to solid tumors. Adv Drug Deliv Rev. 2008; 60:1193–1208. [PubMed: 18474406]
31. Camera L, Kinuya S, Garmestani K, Pai LH, Brechbiel MW, Gansow OA, Paik CH, Pastan I, Carrasquillo JA. Evaluation of a new DTPA-derivative chelator: comparative biodistribution and imaging studies of 111In-labeled B3 monoclonal antibody in athymic mice bearing human epidermoid carcinoma xenografts. Nucl Med Biol. 1993; 20:955–962. [PubMed: 8298575]
32. Yao Z, Zhang M, Axworthy DB, Wong KJ, Garmestani K, Park L, Park CW, Mallett RW, Theodore LJ, Yau EK, Waldmann TA, Brechbiel MW, Paik CH, Pastan I, Carrasquillo JA. Radioimmunotherapy of A431 xenografted mice with pretargeted B3 antibody-streptavidin and (90)Y-labeled 1,4,7,10-tetraazacyclododecane-N, N′, N″, N‴ -tetraacetic acid (DOTA)-biotin. Cancer Res. 2002; 62:5755–5760. [PubMed: 12384535]
33. O'Neill BE, Vo H, Angstadt M, Li KP, Quinn T, Frenkel V. Pulsed high intensity focused ultrasound mediated nanoparticle delivery: mechanisms and efficacy in murine muscle. Ultrasound Med Biol. 2009; 35:416–424. [PubMed: 19081668]
34. Minchinton AI, Tannock IF. Drug penetration in solid tumours. Nat Rev Cancer. 2006; 6:583–592. [PubMed: 16862189]
35. Dreher MR, Chilkoti A. Toward a systems engineering approach to cancer drug delivery. J Natl Cancer Inst. 2007; 99:983–985. [PubMed: 17596569]
36. O'Brien WD Jr. Ultrasound-biophysics mechanisms. Prog Biophys Mol Biol. 2007; 93:212–255. [PubMed: 16934858]
37. Frenkel V, Etherington A, Greene M, Quijano J, Xie J, Hunter F, Dromi S, Li KC. Delivery of liposomal doxorubicin (Doxil) in a breast cancer tumor model: investigation of potential enhancement by pulsed-high intensity focused ultrasound exposure. Acad Radiol. 2006; 13:469–479. [PubMed: 16554227]
38. Patel PR, Luk A, Durrani A, Dromi S, Cuesta J, Angstadt M, Dreher MR, Wood BJ, Frenkel V. In vitro and in vivo evaluations of increased effective beam width for heat deposition using a split focus high intensity ultrasound (HIFU) transducer. Int J Hyperthermia. 2008; 24:537–549. [PubMed: 18608578]
39. Sheikov N, McDannold N, Vykhodtseva N, Jolesz F, Hynynen K. Cellular mechanisms of the blood-brain barrier opening induced by ultrasound in presence of microbubbles. Ultrasound Med Biol. 2004; 30:979–989. [PubMed: 15313330]
40. Baxter LT, Jain RK. Transport of fluid and macromolecules in tumors. I. Role of interstitial pressure and convection. Microvasc Res. 1989; 37:77–104. [PubMed: 2646512]
41. Watson KD, Lai CY, Qin S, Kruse DE, Lin YC, Seo JW, Cardiff RD, Mahakian LM, Beegle J, Ingham ES, Curry FR, Reed RK, Ferrara KW. Ultrasound increases nanoparticle delivery by reducing intratumoral pressure and increasing transport in epithelial and epithelial-mesenchymal transition tumors. Cancer Res. 2012; 72:1485–1493. [PubMed: 22282664]
42. van Dieren EB, Plaizier MA, van Lingen A, Roos JC, Barendsen GW, Teule GJ. Absorbed dose distribution of the auger emitters 67GA and 125I and the beta-emitters 67CU, 90Y, 131I, and

186RE as a function of tumor size, uptake, and intracellular distribution. Int J Radiat Oncol Biol Phys. 1996; 36:197–204. [PubMed: 8823276]

43. Sugahara KN, Teesalu T, Karmali PP, Kotamraju VR, Agemy L, Greenwald DR, Ruoslahti E. Coadministration of a tumor-penetrating peptide enhances the efficacy of cancer drugs. Science. 2010; 328:1031–1035. [PubMed: 20378772]
44. Jang SH, Wientjes MG, Au JL. Enhancement of paclitaxel delivery to solid tumors by apoptosis-inducing pretreatment: effect of treatment schedule. J Pharmacol Exp Ther. 2001; 296:1035–1042. [PubMed: 11181938]
45. Goodman TT, Olive PL, Pun SH. Increased nanoparticle penetration in collagenase-treated multicellular spheroids. Int J Nanomedicine. 2007; 2:265–274. [PubMed: 17722554]
46. Eikenes L, Bruland OS, Brekken C, Davies Cde L. Collagenase increases the transcapillary pressure gradient and improves the uptake and distribution of monoclonal antibodies in human osteosarcoma xenografts. Cancer Res. 2004; 64:4768–4773. [PubMed: 15256445]
47. Wong C, Stylianopoulos T, Cui J, Martin J, Chauhan VP, Jiang W, Popovic Z, Jain RK, Bawendi MG, Fukumura D. Multistage nanoparticle delivery system for deep penetration into tumor tissue. Proc Natl Acad Sci U S A. 2011; 108:2426–2431. [PubMed: 21245339]
48. Grainger SJ, Serna JV, Sunny S, Zhou Y, Deng CX, El-Sayed ME. Pulsed ultrasound enhances nanoparticle penetration into breast cancer spheroids. Mol Pharm. 2010; 7:2006–2019. [PubMed: 20957996]

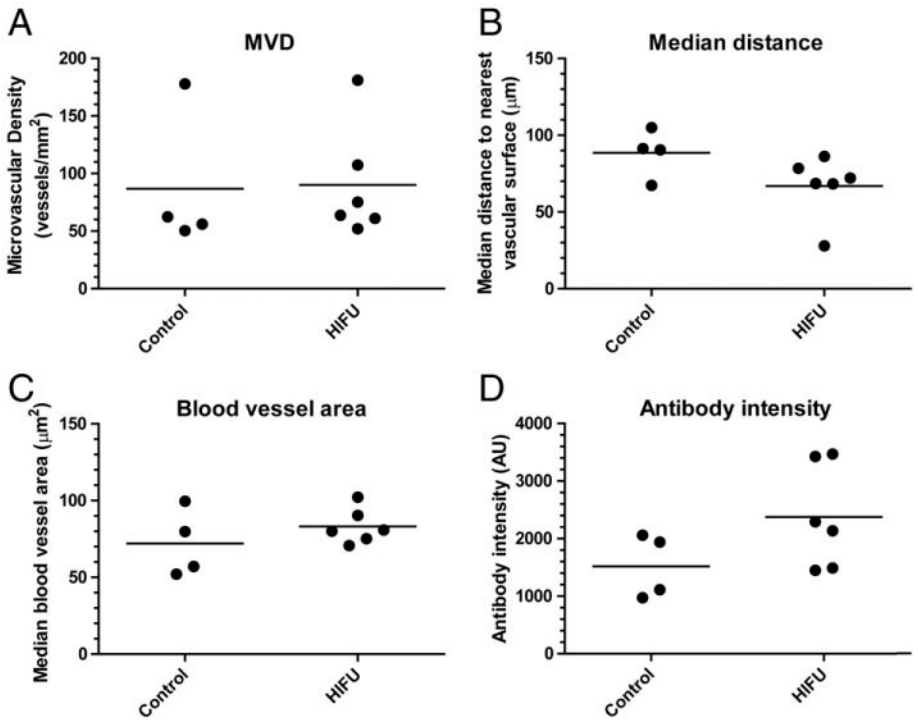

Fig. 1.

Tumor microvascular and antibody accumulation analysis of A431 tumors following treatment with HIFU and Alexa-647-B3. A) Tumor microvascular density (MVD) indicating overall spatial density of tumor microvasculature. B) Median distance from a tumor cell to the nearest vascular surface that describes overall microvascular architecture with smaller distances more efficient for transport. C) Blood vessel area to indicate blood vessel size, and D) Overall antibody intensity in the entire tumor section demonstrating the accumulation of antibody. Data are presented as individual data points and the bar represents the (n = 4–6).

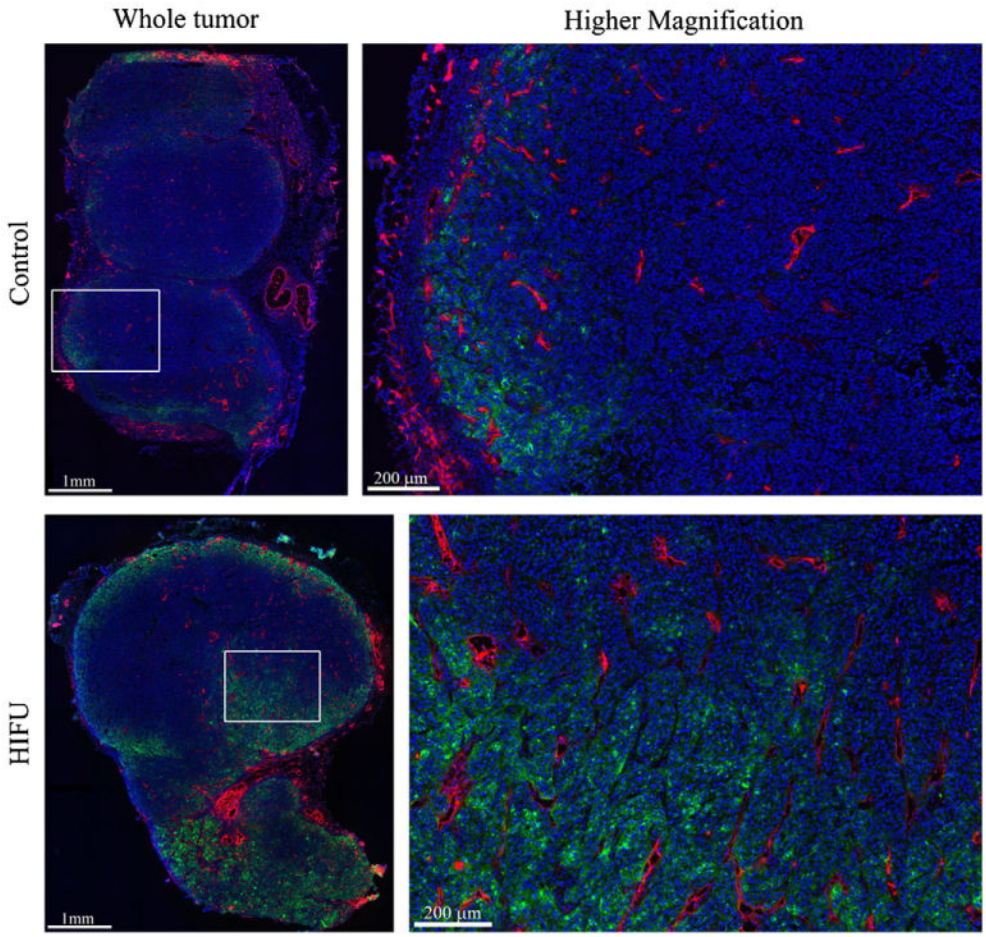

Fig. 2.

Fluorescence images of antibody distribution. Alexa-647-B3 antibody (green), blood vessels (red), and nuclei (blue) are shown for each group as a whole tumor (left column) and with higher magnification (right column). The white box corresponds to the region displayed in the right column. The Alexa-647-B3 antibody channel was acquired and displayed with consistent levels, while the blood vessels and nuclei are displayed to maximize contrast.

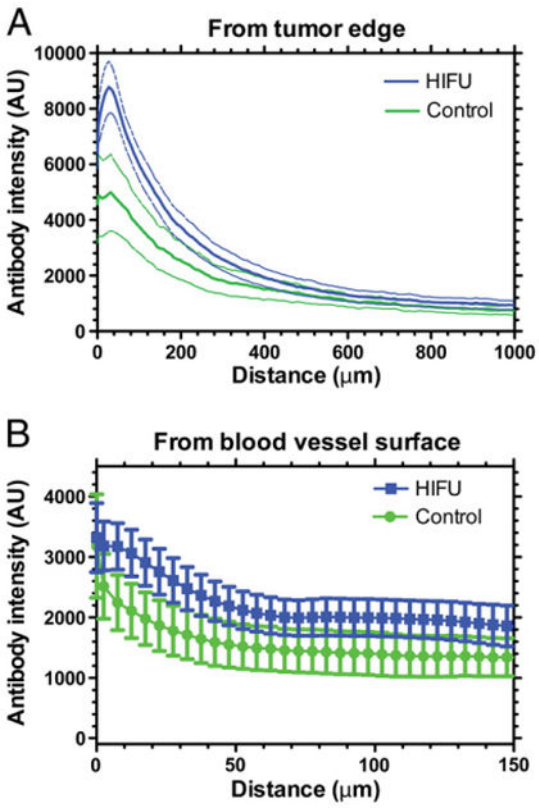

Fig. 3.

Antibody penetration from the tumor edge (A) and blood vessel surface (B). Data are mean ±SEM shown as a dashed line (A) or error bars (B), n=4–6. Control and HIFU are significantly different from the tumor edge up to 50 μm.

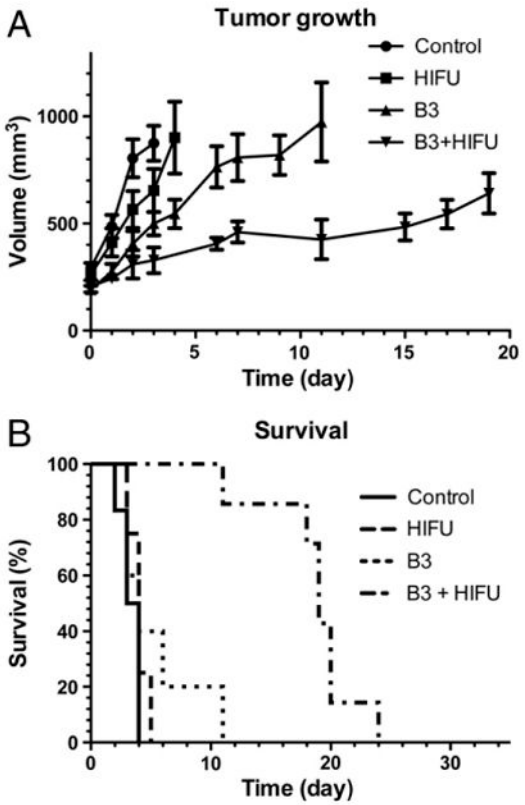

Fig. 4.

Tumor growth (A) and survival (B) shown as a Kaplan–Meier plot. A) Tumor growth is delayed by treatment with ^{90}Y-B3 and ^{90}Y-B3+HIFU (mean±SD). B) Survival is extended by treatment with ^{90}Y-B3+HIFU versus all other groups (p-value < 0.05).